Rapid Communications

Experimental observation of Faraday waves in soft gels

X. Shao,[1] G. Bevilacqua,[2] P. Ciarletta,[2] J. R. Saylor,[1] and J. B. Bostwick[1]
[1]*Department of Mechanical Engineering, Clemson University, Clemson, 29634 South Carolina, USA*
[2]*MOX, Dipartimento di Matematica, Politecnico di Milano, Piazza Leonardo da Vinci 32, Milano, Italy*

(Received 7 August 2020; accepted 4 December 2020; published 23 December 2020)

We report the experimental observation of Faraday waves on soft gels. These were obtained using agarose in a mechanically vibrated cylindrical container. Low driving frequencies induce subharmonic standing waves with spatial structure that conforms to the geometry of the container. We report the experimental observation of the first 15 resonant Faraday wave modes that can be defined by the mode number (n, ℓ) pair. We also characterize the shape of the instability tongue and show the complex dependence upon material properties can be understood as an elastocapillary effect.

DOI: 10.1103/PhysRevE.102.060602

Faraday waves [1] are a paradigm for pattern formation on interfaces and have been used to study nonlinear and emergent phenomena in liquids for some time [2,3]. Recent interest in tissue engineering [4] has motivated the use of surface waves to control the assembly of particles [5–7] and organoid cells [8] in bioprinting technologies [9]. These technologies often use soft hydrogels as the working material [10] and require precise spatial and temporal controls of the surface pattern. Much of the work on bioprinting has focused on the use of drop deposition or extrusion of gels to create cell patterns, and there have been comparatively few studies of the formation of surface waves on soft gels [11,12]. In this Rapid Communication, we report the experimental observation of low-frequency Faraday waves on soft gels and characterize the shape of the resonant "instability tongue" which exhibits a complex dependence on the elastocapillary properties of the gel.

Instabilities develop when the energy balance in a system changes from favorable to unfavorable resulting in a bifurcation into a new state. For Faraday waves on liquids, there is a competition between the mechanical energy supplied by vibration, the restorative energy of surface tension, and dissipation due to viscosity. When this balance becomes unfavorable, i.e., when the mechanical energy outweighs dissipation, a standing wave emerges on the surface of the liquid. Benjamin and Ursell [13] showed that Faraday waves occur inside the instability tongues (neutral stability curves) of the Mathieu equation and that the surface wave dynamics could be subharmonic (half the driving frequency), harmonic (equal to the driving frequency), or superharmonic (multiples of the driving frequency). Most studies of Faraday waves focus on the subharmonic response as the corresponding onset acceleration is typically smaller than that for the harmonic and superharmonic tongues. However, there are exceptions including the case of a thin viscous layer which exhibits a harmonic response due to high dissipation that dramatically increases the onset acceleration of the subharmonic tongue relative to the harmonic one [14,15]. The role of the container geometry on the spatial structure of the standing wave is largely determined by the wavelength relative to the container size; high driving frequencies generate waves with a continuous wave number such that container geometry is irrelevant [16], whereas low driving frequencies excite waves that conform to the container boundary and are described by an integer-valued mode number pair exhibiting a finite bandwidth [17–20]. Near the boundary between two modes, nonlinear mode-mode interactions become important, and chaos has been observed [21,22]. Our experiments are performed for low driving frequencies and generate Faraday waves that respect the symmetry of the cylindrical container as shown in Fig. 1.

Gels differ from liquids in that they possess a finite elasticity that must enter into the energy balance [23]. We are interested in how the shape of the instability tongue changes with elasticity. For soft gels, surface tension and elasticity are of comparable magnitude as defined by the elastocapillary number $\Sigma = \sigma/RG$, where σ is the surface tension, G is the shear modulus, and R is the characteristic length scale [24,25]. For our experiments, R is the radius of the cylindrical container, and we explore the range of elastocapillary number $\Sigma = 0.16$–7.62 that encompasses a transition at $\Sigma \sim 1$ between capillary and elastic wave behavior. Recent experiments have shown that soft gels $G \sim 10$ Pa are susceptible to capillary instabilities, such as elastocapillary waves [11,12], Plateau-Rayleigh breakup of a cylinder [26], Rayleigh-Taylor instability of an elastic layer [27,28], and Rayleigh gel drop oscillations [29,30]. Faraday waves also belong to the canon of hydrodynamic instabilities but have not been observed on soft gels, to our knowledge. We note in passing that Faraday waves on liquids can exhibit significant surface streaming and particle motion, an important part of the literature in this area [31–34]; such motions cannot be seen in gels due to the absence of lateral surface motion.

Experiment. Gels are made by dissolving agarose powder (Sigma-Aldrich Type VI-A) in doubly distilled water at 90° C for 1 h to form a solution which is then poured into a cylindrical plexiglass container of radius $R = 35$ mm and height

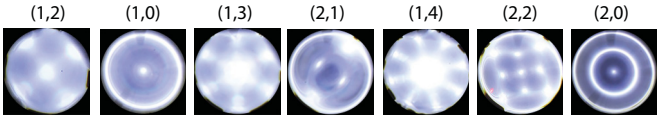

FIG. 1. Experimentally observed surface modes with mode number pair (n, ℓ) on a gel with $G = 3.9$ Pa.

$H = 22$ mm [35]. The range of concentrations explored was $\phi = 0.038$–0.105 wt%. A syringe is used to either add or subtract solution prior to gelation in order to create a pinned contact line with contact angle $\alpha = 90^\circ$. This procedure is known to eliminate undesirable harmonic edge waves, at least, for liquids. The container is then covered to minimize evaporation, and the solution is allowed to gel at room temperature for 3 h or more. The gel rheology is defined by the complex modulus $G' + iG''$ and measured using oscillatory tests with an Anton Paar MCR 302 rheometer. The loss modulus G'' is generally, at least, an order of magnitude smaller than the storage modulus G', and we, therefore, assume our gels behave as an elastic solid defined by the shear modulus $G \equiv G'$ [35]. The range of shear modulus explored was $G = 0.27$–12.2 Pa. Because the concentration of agarose solution is so dilute, we assume the density $\rho = 1.0$ g/mL and surface tension $\sigma = 72$ mN/m, viz. the same as that of water.

Faraday waves are excited in experiment using the setup shown in Fig. 2(a). The cylindrical container which holds the gel is mounted on a Labworks ET-139 electromechanical shaker which provides vertical vibration of the tank. The shaker is driven by an Agilent 33220A function generator and Labworks PA-141 amplifier combination over a range of frequencies $f_d = 7$–29 Hz. The forcing amplitude of the shaker A was measured using a PCB 352C33 accelerometer and a PCB 482C05 signal conditioner combination, where A is the max-min of the sinusoidal acceleration signal.

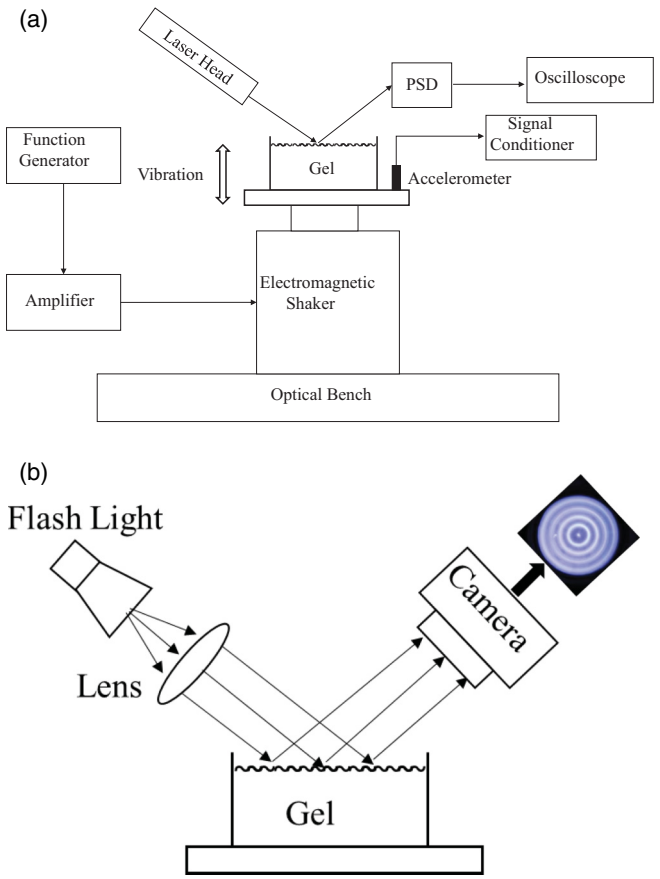

FIG. 2. Schematic of (a) experimental setup and (b) optical system.

To detect the onset of Faraday waves and the corresponding surface wave frequency, we use a laser light system consisting a helium neon laser beam (632.8 nm wavelength) that is directed at the free surface and reflected to a position sensitive detector (PSD), which produces an analog voltage signal proportional to the position of the laser beam striking the sensor. This signal is processed via a fast Fourier transform (FFT) operation on an oscilloscope, giving the surface wave frequency. In our experiments, the observed frequency f_o is half of the driving frequency $f_o = 0.5 f_d$, consistent with the subharmonic response of Faraday waves. For fixed driving frequency f_d, the Faraday wave threshold is approached by increasing the output amplitude from the amplifier until the rapid growth of a frequency peak at $f_o = 0.5 f_d$ is observed on the FFT. This gives the upper limit A_u for the threshold amplitude at that particular driving frequency. We then decrease the output amplitude until the frequency peak disappears on the FFT giving the lower threshold amplitude A_l. The true threshold acceleration lies within the interval $[A_l, A_u]$, and we iterate the above protocol until $A_u - A_l \leqslant 0.2$ m/s^2 after which we define $A = (A_u + A_l)/2$ as the experimental threshold amplitude for Faraday wave onset.

The optical system shown in Fig. 2(b) is used to characterize the spatial structure of the surface wave. Collimated light is produced by a lens located one focal length $f = 300$ mm from a white light emitting diode flashlight. A plate with a 2 mm diameter hole is placed in front of the light to approximate a point light source. The resulting collimated beam is directed at the wave surface and the reflected light captured by a digital camera (Canon EOS Rebel T3i with a Canon EF-S 18-55 mm lens) oriented so its optical axis is parallel to the direction of the reflected white light. A long exposure time $t = 0.8$ s is used to generate experimental images of the wave patterns (cf. Fig. 1). Here the locations where the wave slope is zero (i.e., the peaks or troughs) are bright, whereas the regions where the wave slope is nonzero (e.g., the nodes) appear dark with larger slopes yielding darker pixel intensities.

For the low driving frequencies used in our experiment, the surface waves conform to the boundary of the cylindrical container and are described by an integer-valued mode number pair [17,19]. This is in contrast to high-frequency waves which exhibit a continuous wave number and are insensitive to the container boundary [16]. To identify the modal structure, we use a two dimensional cross correlation between the experimental wave pattern and a Bessel function $J_\ell(k_n r)\cos(\ell\theta)$ with ℓ as the azimuthal mode number and k_n computed from the roots of $J'_\ell(k_n R) = 0$, where n is the numerical order of those roots. For each experimental image, the mode number is taken as the (n, ℓ) pair where the cross correlation is maximized. This procedure was used to identify the mode numbers for the images presented herein.

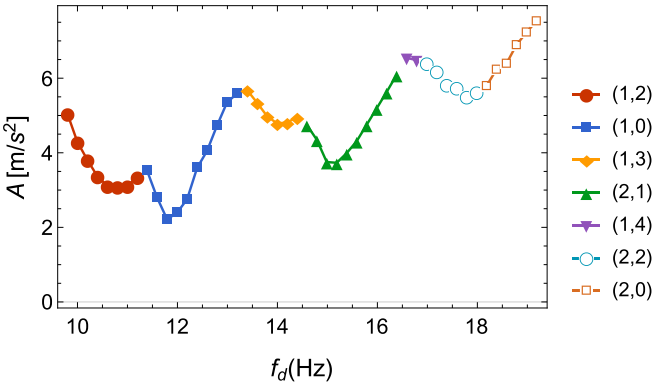

FIG. 3. Frequency sweep plotting acceleration A against driving frequency f_d for $G = 3.9$ Pa reveals instability tongues for modes (n, ℓ).

Results. A typical frequency sweep is shown in Fig. 3 for a gel with $G = 3.9$ Pa. Multiple modes are observed with their corresponding instability tongues plotted in the acceleration-frequency space. Broadly speaking, the accelerations increase with frequency. Most modes, e.g., (1,2), (1,0), (1,3), (2,1), and (2,2), exhibit a full instability tongue with a local minimum that one can associate with the resonance frequency for that particular mode and a finite bandwidth [13]. Some modes, e.g., (1,4) and (2,0), only display a partial tongue which we believe is due to mode competition for these driving frequencies. That is, the respective instability tongues overlap causing mode-mode interactions that have been shown to exhibit nonlinear effects, such as hysteresis and chaotic dynamics [21,22] thereby precluding experimental identification of a clear and complete instability tongue. As the frequency increases, the overlap of modes becomes more significant and the range of frequencies over which a given mode can be excited decreases. For example, the (1,4) mode can only be observed over a particularly small frequency range $\Delta f_d = 0.4$ Hz (cf. Fig. 3). Despite this fact, we have experimentally observed the first 15 resonant Faraday wave modes on a gel with $G = 5.9$ Pa as shown in Fig. 4 which shows the surface structure

	$\ell = 0$	1	2	3	4	5
$n = 1$	11.6-13.4 Hz	7.0-9.0 Hz	9.2-11.4 Hz	13.6-14.2 Hz	17.1 Hz	
2	18.8-20.0 Hz	14.4-16.8 Hz	17.2-18.6 Hz	20.2-21.6 Hz	23.4-24.4 Hz	26.8-27.8 Hz
3	25.8-26.6 Hz	21.8-23.2 Hz	24.6-25.6 Hz	28.0-28.6 Hz		

FIG. 4. Table of experimentally observed Faraday wave mode shapes on a gel with $G = 5.9$ Pa defined by the mode number pair (n, ℓ) with a corresponding frequency range.

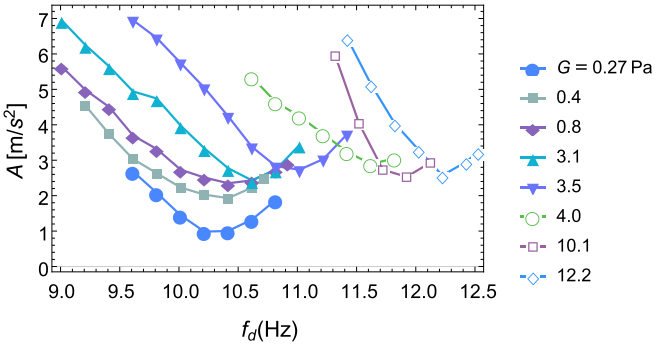

FIG. 5. Instability tongue for the (1,2) mode in the acceleration A versus frequency f_d space as it depends upon shear modulus G.

of each of the 15 modes as well as the corresponding driving frequency range.

The low-frequency modes show the least degree of overlap and are, therefore, most suitable to explore the role of elasticity on the shape of the instability tongue for a pure mode. The lowest-frequency mode is the (1,1) sloshing mode. However, the motion of the surface is large for this mode, making the detection of onset difficult. For this reason, we investigate the (1,2) mode which is the next highest-frequency mode. Figure 5 is a plot of the instability tongue for the (1,2) mode as it depends upon the shear modulus G. A complete instability tongue is observed in each case with significantly smaller high-frequency side due to the interaction with the (1,0) mode. The resonance frequency shows a monotonic increase with G, whereas the threshold acceleration asymptotically approaches a maximum value.

This dependence upon the material parameters can be understood by dimensional analysis and examining limiting behavior. For gels, the relative importance of surface tension to elasticity is given by the elastocapillary number $\Sigma \equiv \sigma/RG$, which for our experiments lies in the range of $\Sigma = 0.16$–7.62. Here $\Sigma \to 0$ and $\Sigma \to \infty$ correspond to the elastic and capillary limits, respectively. As we have performed in our prior work on hydrogels, we hypothesize that the elastic and capillary forces act in parallel [29,36]. Faraday wave onset is then determined by the total resistance R_T to wave motion, which can be written as $\frac{1}{R_T} = \frac{1}{R_\sigma} + \frac{1}{R_G}$, where R_σ is the resistance of surface motion due to capillarity, and R_G is the resistance to surface motion due to elasticity. Given that the elastocapillary number Σ is the ratio of capillary to elastic forces, the total resistance becomes $R_t = \frac{R_\sigma}{1+\Sigma}$. Assuming σ and, hence, R_σ are constant, we expect R_t to asymptotically approach a constant as $\Sigma \to 0$ and to approach zero as $\Sigma \to \infty$. This is precisely what the threshold acceleration behavior shows in Fig. 5. Furthermore, the resonance frequency monotonically increases with G, consistent with prior work for gel drops [36], suggesting our interpretation of the physics is sound.

Discussion. We have reported the first experimental observation of Faraday waves in soft gels having observed the first 15 resonant modes and characterized the shape of the instability tongue for the most repeatable (1,2) mode. By exploring a range of gel elasticities we are able to capture the elastocapillary transition between elastic-dominated and

capillary-dominated Faraday waves (cf. Fig. 5) in this canonical problem in pattern formation.

There is a long history of using Faraday waves to pattern the surface of granular media [37], surfactant-laden [38] and particle-laden [7] thin films, and bioinks with organelles [8]. Numerous technologies exploit pattern formation in Faraday waves on liquids including pinchoff in inkjet printing [39], and drop atomization (aerosols) for drug delivery [40,41]. Our results can be useful for controlling the spatial and temporal evolutions of cell-laden bioinks (during the gelling process) used in cell printing technologies [42] where complex tissue scaffold architectures are desired. In fact, it may be possible to pattern multiple cells into a predetermined Faraday wave pattern, such as those we observe in our experiments (cf. Fig. 1).

We have observed more complex spatial patterns which couple edge waves and Faraday waves using water as the working material. This is performed by purposefully controlling the meniscus geometry such that the contact angle of $\alpha < 90^\circ$. For these experimental conditions, it is possible to excite an axisymmetric $(n, 0)$ harmonic edge wave and azimuthal (n, ℓ) subharmonic Faraday wave at the same driving frequency above the Faraday wave acceleration threshold. These motions exhibit both spatial and temporal complexities, and we would expect nonlinear effects, such as hysteresis and chaos [21,22], to become particularly important near the boundary between adjoining instability tongues due to the triad mode-mode-mode interactions between the edge wave mode and two adjoining Faraday wave modes.

Finally, we mention that the agarose gels we use in our experiments exhibit a relatively simple rheology, i.e., they have a constant elasticity (storage modulus) and relatively low viscosity (loss modulus) over the range of frequencies explored. This choice of material was intentional in order to explore the physics of elastocapillarity in Faraday waves in the absence of a complex frequency-dependent rheology. Our results show we have a good understanding of this system. Soft gels with a more complex rheology will exhibit a relaxation timescale and these additional physics should affect pattern formation and the shape of the instability tongues. This should be pursued further in future studies.

Acknowledgments. J.B.B. acknowledges support from NSF Grant No. CBET-1750208. G.B. and P.C. acknowledge support from MIUR, PRIN 2017, and Research Project No. 2017KL4EF3.

[1] M. Faraday, Philos. Trans. R.l Soc. London **121**, 299 (1831).
[2] J. Miles and D. Henderson, Annu. Rev. Fluid Mech. **22**, 143 (1990).
[3] M. Perlin and W. W. Schultz, Annu. Rev. Fluid Mech. **32**, 241 (2000).
[4] S. Guven, P. Chen, F. Inci, S. Tasoglu, B. Erkmen, and U. Demirci, Trends Biotechnol. **33**, 269 (2015).
[5] P. Chen, Z. Luo, S. Güven, S. Tasoglu, A. V. Ganesan, A. Weng, and U. Demirci, Adv. Mater. **26**, 5936 (2014).
[6] J. Saylor and A. Kinard, Phys. Fluids **17**, 047106 (2005).
[7] P. Wright and J. Saylor, Rev. Sci. Instrum. **74**, 4063 (2003).
[8] P. Chen, S. Güven, O. B. Usta, M. L. Yarmush, and U. Demirci, Adv. Healthcare Mater. **4**, 1937 (2015).
[9] R. Suntornnond, J. An, and C. K. Chua, Macromolecular Materials and Engineering **302**, 1600266 (2016).
[10] S. Ji and M. Guvendiren, Front. Bioeng. Biotechnol. **5**, 23 (2017).
[11] F. Monroy and D. Langevin, Phys. Rev. Lett. **81**, 3167 (1998).
[12] X. Shao, J. R. Saylor, and J. B. Bostwick, Soft Matter **14**, 7347 (2018).
[13] T. B. Benjamin and F. J. Ursell, Proc. R. Soc. London, Ser. A **225**, 505 (1954).
[14] K. Kumar, Proc. R. Soc. London, Ser. A **452**, 1113 (1996).
[15] H. W. Müller, H. Wittmer, C. Wagner, J. Albers, and K. Knorr, Phys. Rev. Lett. **78**, 2357 (1997).
[16] W. S. Edwards and S. Fauve, J. Fluid Mech. **278**, 123 (1994).
[17] D. M. Henderson and J. W. Miles, J. Fluid Mech. **213**, 95 (1990).
[18] S. Douady and S. Fauve, Europhys. Lett. **6**, 221 (1988).
[19] S. Douady, J. Fluid Mech. **221**, 383 (1990).
[20] W. Batson, F. Zoueshtiagh, and R. Narayanan, J. Fluid Mech. **729**, 496 (2013).
[21] S. Ciliberto and J. P. Gollub, Phys. Rev. Lett. **52**, 922 (1984).
[22] S. Ciliberto and J. Gollub, J. Fluid Mech. **158**, 381 (1985).
[23] M. Rubinstein and R. Colby, *Polymer Physics* (Oxford University Press, Oxford, 2003).
[24] R. W. Style, A. Jagota, C.-Y. Hui, and E. R. Dufresne, Annu. Rev. Condens. Matter Phys. **8**, 99 (2017).
[25] J. Bico, É. Reyssat, and B. Roman, Annu. Rev. Fluid Mech. **50**, 629 (2018).
[26] S. Mora, T. Phou, J.-M. Fromental, L. M. Pismen, and Y. Pomeau, Phys. Rev. Lett. **105**, 214301 (2010).
[27] S. Mora, T. Phou, J.-M. Fromental, and Y. Pomeau, Phys. Rev. Lett. **113**, 178301 (2014).
[28] Y. Zheng, Y. Lai, Y. Hu, and S. Cai, J. Mech. Phys. Solids **131**, 221 (2019).
[29] X. Shao, S. A. Fredericks, J. R. Saylor, and J. B. Bostwick, Phys. Rev. Lett. **123**, 188002 (2019).
[30] S. Tamim and J. Bostwick, Soft Matter **15**, 9244 (2019).
[31] R. Ramshankar, D. Berlin, and J. P. Gollub, Phys. Fluids A **2**, 1955 (1990).
[32] N. Francois, H. Xia, H. Punzmann, S. Ramsden, and M. Shats, Phys. Rev. X **4**, 021021 (2014).
[33] G. Vuillermet, P.-Y. Gires, F. Casset, and C. Poulain, Phys. Rev. Lett. **116**, 184501 (2016).
[34] N. Perinet, P. Gutierrez, H. Urra, and N. Muica, J. Fluid Mech. **819**, 285 (2017).
[35] M. Tokita and K. Hikichi, Phys. Rev. A **35**, 4329 (1987).
[36] X. Shao, S. Fredericks, J. Saylor, and J. Bostwick, J. Acoust. Soc. Am. **147**, 2488 (2020).
[37] F. Melo, P. Umbanhowar, and H. L. Swinney, Phys. Rev. Lett. **72**, 172 (1994).
[38] S. L. Strickland, M. Shearer, and K. E. Daniels, J. Fluid Mech. **777**, 523 (2015).

[39] A. James, B. Vukasinovic, M. Smith, and A. Glezer, J. Fluid Mech. **476**, 1 (2003).

[40] B. Vukasinovic, M. Smith, and A. Glezer, J. Fluid Mech. **587**, 395 (2007).

[41] C. Tsai, R. Mao, S. Lin, Y. Zhu, and S. Tsai, Technology **2**, 75 (2014).

[42] U. Demirci and G. Montesano, Lab Chip **7**, 1139 (2007).